

Characterizing the mixed eigenstates in kicked top model through the out-of-time-order correlator

Qian Wang 

*CAMTP-Center for Applied Mathematics and Theoretical Physics,
University of Maribor, Mladinska 3, SI-2000 Maribor, Slovenia, and
Department of Physics, Zhejiang Normal University, Jinhua 321004, China*

Marko Robnik 

*CAMTP-Center for Applied Mathematics and Theoretical Physics,
University of Maribor, Mladinska 3, SI-2000 Maribor, Slovenia*

(Dated: March 4, 2025)

Generic systems are associated with a mixed classical phase space. The question of the properties of the eigenstates for these systems remains less known, although it plays a key role for understanding several important quantum phenomena such as thermalization, scarring, tunneling, and (de-)localization. In this work, by employing the kicked top model, we perform a detailed investigation of the dynamical signatures of the mixed eigenstates via the out-of-time-order correlator (OTOC). We show how the types of the eigenstates get reflected in the short- and long-time behaviors of the OTOC and conjecture that the dynamics of the OTOC can be used as an indicator of the mixed eigenstates. Our findings further confirm the usefulness of the OTOC for studying quantum complex systems and also provide more insights into the characters the mixed eigenstates.

I. INTRODUCTION

Studying dynamical properties of eigenstates in quantum many-body systems has attracted much attention in modern science, due to their crucial role for understanding numerous fundamental questions arisen in different research areas, including quantum chaos [1–5], statistical mechanics [3, 4], and condensed matter physics [6, 7]. Moreover, the endeavor to investigate the dynamical features of eigenstates in quantum systems is also pivotal for various applications of quantum-based techniques, such as quantum simulation [8, 9] and metrology [10, 11].

Numerous works have been devoted to investigating the dynamical signatures of eigenstates in the fully chaotic systems, see e. g. Refs. [3–5] and references therein. However, a generic many-body system is neither regular nor fully chaotic. Instead, it behaves as a mixed-type system. Pretty much different from both regular and strong chaotic cases, the mixed-type systems are characterized by the coexistence of regular islands and chaotic regions in phase space of their classical counterparts. Hence, the quest to classify the eigenstates in mixed-type systems is important for studying them.

Percival in his seminal work [12] proposed to classify the spectra of quantum mixed-type systems into regular and chaotic eigenstates, supported, respectively, by invariant tori in regular islands and chaotic seas in corresponding classical phase space [13]. This proposal has been further developed by Berry and coworkers [14, 15] and finally leads to the so-called principle of uniform semiclassical condensation (PUSC) of Wigner (or Husimi) functions [16]. This is the basis for the Berry-Robnik picture regarding the statistical properties of the energy spectra, the level spacings distribution [17]. See Refs. [18, 19] and references therein for more details about the PUSC.

Although the binary separation of quantum eigenstates has been verified and commonly accepted in the studies of quantum chaos, the picture for reality situations is more complicated. Actually, the sharp distinction between chaotic and regular eigenstates only happens in the ultimate semiclassical limit. Moreover, it is known that different phase space structures of mixed-type systems can be connected through various tunneling processes [20–22]. These facts strongly indicate that the mixed-type systems also allow their eigenstates behaving as mixed states. In contrast to the regular and fully chaotic eigenstates, the Husimi function of mixed eigenstates is distributed in both regular and chaotic regions [23–25]. This raises a natural and intriguing question: what are the properties of the mixed eigenstates? Previous works have examined their statistical properties [26] and how their relative fraction decreases as the semiclassical limit is approached [23–25, 27, 28] in several mixed-type systems. However, a detailed understanding of their dynamical features is still lacking in current studies.

In the present work, we make a step toward addressing this question. To this end, we carry out a thorough analysis of the dynamical signatures of the mixed eigenstates in quantum kicked top model by means of the out-of-time-order correlators (OTOCs). As a measure of quantum information scrambling [29–32], the concept of OTOC was first introduced for the semiclassical study of superconductivity [33] and, recently, it has been commonly used in condensed matter [34–37] and high-energy physics [38, 39]. In particular, they exhibit an initial exponential growth behavior for the quantum systems with chaotic classical counterpart [40–43], leading to the so-called quantum butterfly effect

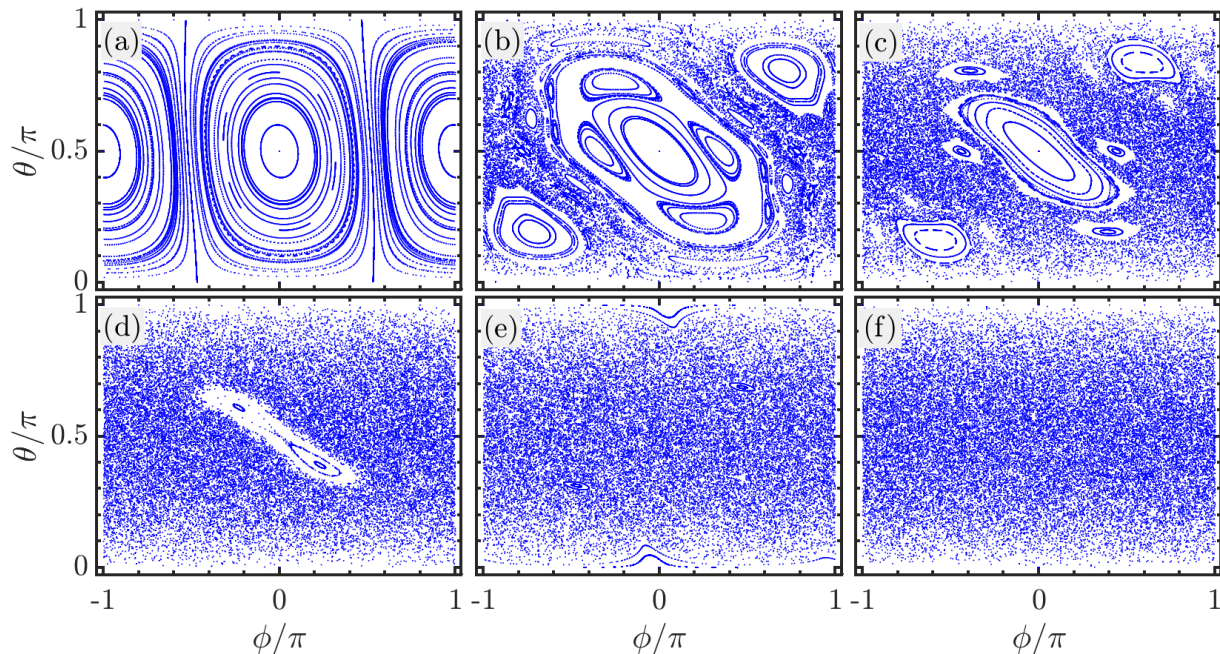


FIG. 1. Classical phase space portraits of the kicked top model for 121 random initial conditions with $\kappa = 0.2, 2.2, 3, 4.3, 6,$ and $\kappa = 7$ [from (a) to (f)]. Each initial condition has been evolved for 300 kicks. Other parameter: $\alpha = 13\pi/19$.

[44, 45]. As a result, the OTOCs have been recognized as the quantum analogue of classical instability with respect to initial condition. This triggers a vast amount of studies on the connections between OTOCs and quantum chaos [46–56]. However, it should be emphasized that such exponential instability occurs only at finite time (i. e. Ehrenfest time), unlike the classical case with positive Lyapunov exponents. Moreover, the experimental measurement of OTOCs has been accomplished by several platforms [57–61].

The main interest of this work is to explore how the mixed eigenstates get manifested in the evolution of OTOC. We thus focus on the eigenstate expectation values of OTOC, which enables us to analyze the dependence of the behavior of OTOC on the type of eigenstates. We demonstrate that the mixed feature of the eigenstates results in strong impact on the evolution of OTOC and discuss how to reveal the dynamical signatures of mixed eigenstates via the properties of OTOC. Specifically, we show that the phase space overlap of the mixed eigenstates correlates with both short-time growth rate and long-time average of the OTOC.

The rest of the article is structured as follows. In Sec. II, we introduce some basic concept of the OTOCs; we provide a short review of the kicked top model, and briefly recall the definition and characterization of the mixed eigenstates. Afterwards, we will report and discuss our results in Sec. III, wherein we show how the mixed eigenstates affect the dynamics of the OTOC. We finally draw our conclusions in Sec. IV.

II. BACKGROUNDS

In this section, we introduce the OTOCs and the model studied in this work. We also briefly discuss the definition and characterization of the mixed eigenstates, the main topic of the present work.

A. Out-of-time-order correlators

The OTOCs quantify the information scrambling in quantum many-body systems [32]. They have attracted a great deal of attention from both theoretical [62–64] and experimental [57–59] aspects in recent years. For a system evolved according to the Hamiltonian H , the OTOC of two Hermitian operators A and B is defined as

$$C(t) = \langle [A(t), B]^\dagger [A(t), B] \rangle = -\langle [A(t), B]^2 \rangle, \quad (1)$$

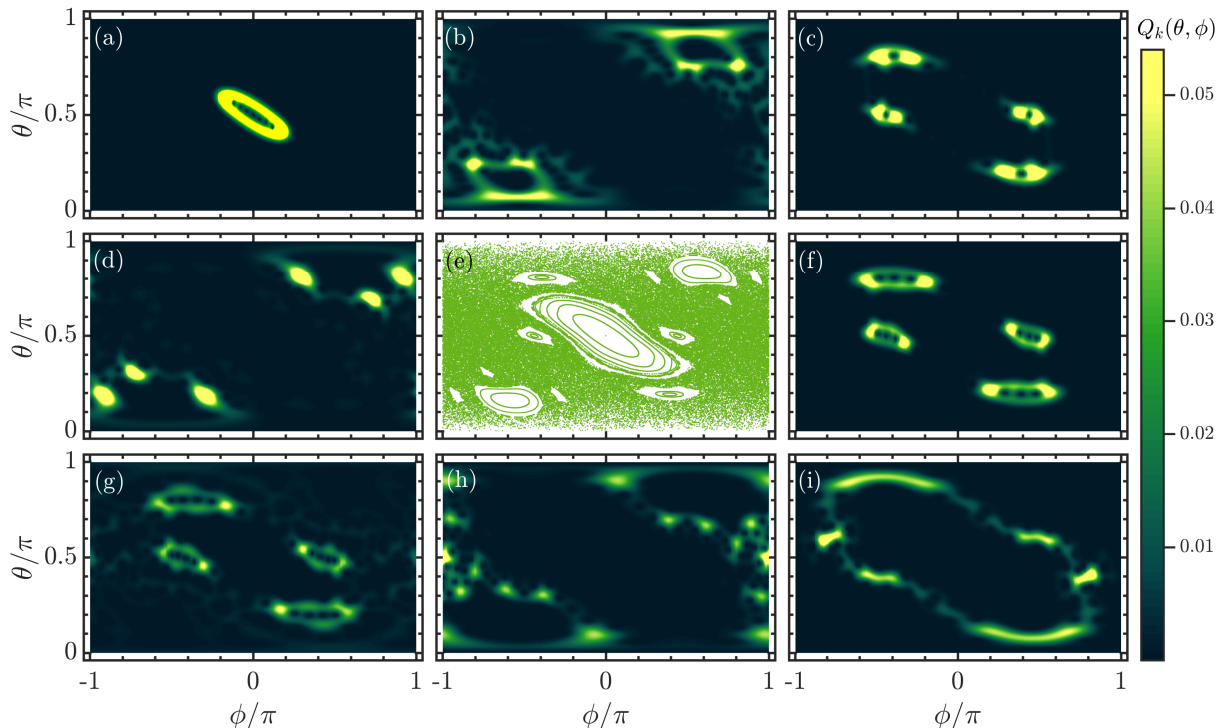


FIG. 2. Husimi function $Q_k(\theta, \phi)$ in (6) for several eigenstates of the Floquet operator with phase space overlap indices are: (a) $\chi_6 = -1$, (b) $\chi_{85} = 0.6371$, (c) $\chi_{113} = -0.275$, (d) $\chi_{147} = 0.5072$, (f) $\chi_{179} = 0.3858$, (g) $\chi_{208} = 0.7262$, (h) $\chi_{230} = 0.9780$, and (i) $\chi_{273} = 0.9985$. The corresponding classical phase portrait is shown in panel (e). Other parameters: $\alpha = 13\pi/19$, $\kappa = 3$, and the system size $S = 150$.

where $A(t) = U^\dagger(t)AU(t)$ with $U(t) = e^{-iHt}$ being the time evolution operator. Here, we set $\hbar = 1$ throughout this work and $\langle \dots \rangle$ denotes an average for certain quantum state. The OTOCs are usually evaluated as thermal average over the canonical ensemble with inverse temperature β [39, 65]. However, in order to reveal the dynamical property of a single state, we consider $C(t)$ as an expectation value for a fixed eigenstate of the system, namely the so called microcanonical OTOC [42, 54, 65].

Although the quantum-classical correspondence [33, 45] implies that a general OTOC increases exponentially with time until the well-known Ehrenfest (or scrambling) time for the quantum system with classical chaotic counterpart [40, 42, 55], whether the OTOC can be used as a dynamical indicator of quantum chaos is still under debate [47–49, 66–70]. Nonetheless, the OTOC analysis could provide more insights into the dynamical features of both isolated [71–78] and open [79–83] quantum systems. OTOC is also widely used for studying the thermalization [84, 85] and acts as a valuable detector of various phase transitions [86–92]. At this point, we would like to mention that the properties of OTOC are obviously dependent on the kind of the observables. They are usually the physically relevant observables, such as the position and momentum operators, as well as spin and particle density operators in finite-range interacting systems. But, the choice of them is usually motivated by certain specific physical problem.

In the present work, we employ the OTOC to analyze the dynamical signatures of the mixed eigenstates in the kicked top model. Before delving into this question and focusing on specific dynamical behaviors, let us provide a brief review on the basic features of the kicked top model and the characterization of the mixed eigenstates.

B. Kicked top model

The kicked top model is a prototypical model in the studies of quantum chaos [93] and can be experimentally realized in different platforms [94–97]. Its quantum version is described by the Hamiltonian

$$H = \alpha S_x + \frac{\kappa}{2S} S_z^2 \sum_{n=-\infty}^{+\infty} \delta(t - n). \quad (2)$$

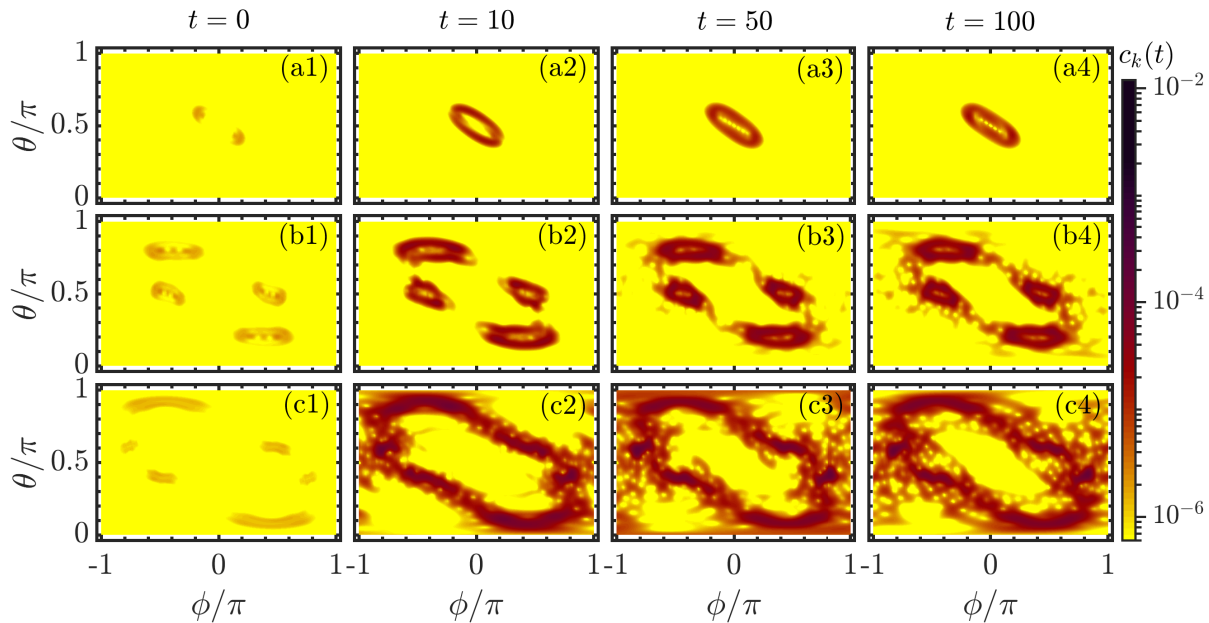


FIG. 3. Snapshots of the OTOC $c_k(t)$, defined in Eq. (10), at different time steps for the eigenstates of the Floquet operator with $\chi_6 = -1$ (a1)-(a4), $\chi_{179} = 0.3858$ (b1)-(b4), and $\chi_{273} = 0.9985$ (c1)-(c4). Other parameters: $\alpha = 13\pi/19$, $\kappa = 3$, and the system size $S = 150$.

Here, S_μ ($\mu = x, y, z$) are the angular momentum operators with total magnitude S and satisfying the standard commutation relations of angular momentum. The parameter α denotes the frequency of the free precession around x axis, while κ represents the strength of periodic δ kicks. As the total angular momentum is a conserved quantity, the Hilbert space of H (2) has finite dimension equal to $2S + 1$. Hence, we can investigate the dynamics of the model without the truncation of the Hilbert space.

It is known that the kick strength κ controls the degree of chaos of the model, indicating a transition from integrability to chaos with increasing κ . This is verified by the quasienergy statistics of the Floquet operator, which governs the time evolution between two successive kicks and is given by

$$\mathcal{F} = \exp\left[-i\frac{\kappa}{2S}S_z^2\right]\exp(-i\alpha S_x). \quad (3)$$

The quasienergy spectrum of H is then obtained through the eigenvalue equation

$$\mathcal{F}|\varepsilon_k\rangle = e^{i\varepsilon_k}|\varepsilon_k\rangle, \quad (4)$$

where ε_k is the k th quasienergy associated to eigenstate $|\varepsilon_k\rangle$.

The presence of chaos in the quantum kicked top model is a manifestation of integrability-to-chaos transition in its classical dynamics, which is given by [98–100]

$$\begin{aligned} X_{m+1} &= X_m \cos \Psi_m - (Y_m \cos \alpha - Z_m \sin \alpha) \sin \Psi_m, \\ Y_{m+1} &= X_m \sin \Psi_m + (Y_m \cos \alpha + Z_m \sin \alpha) \cos \Psi_m, \\ Z_{m+1} &= Y_m \sin \alpha + Z_m \cos \alpha, \end{aligned} \quad (5)$$

where $\Psi_m = \kappa(Y_m \sin \alpha + Z_m \cos \alpha)$ and $\mathbf{X} = (X, Y, Z) = \langle \mathbf{S} \rangle / S$ are the classical dynamical variables. The conservation of \mathbf{S}^2 implies $X^2 + Y^2 + Z^2 = 1$, which allows us to parameterize them as $X = \sin \theta \cos \phi$, $Y = \sin \theta \sin \phi$, and $Z = \cos \theta$, with ϕ and θ being azimuthal and polar angles, respectively. As a result, the classical phase space can be described by canonical variables $\phi = \arctan(Y/X) \in [-\pi, \pi]$ and $\cos \theta \in [-1, 1]$.

A common way to show the transition to chaos in the classical dynamics is to examine the Poincaré section. It was known that the Poincaré section exhibits regular structure for integrable systems, defined by invariant tori, while it consists of randomly scattered points for fully chaotic dynamics. The Poincaré section obtained by solving Eq. (5) for different values of κ with $\alpha = 13\pi/19$ are plotted in Fig. 1. The variation of Poincaré section from regular pattern for

small κ to covered by randomly located points at large κ is clearly indicating the transition to chaos with increasing κ .

Our focus lies on the dynamical signatures of the mixed eigenstates, which exist in the quantum systems with mixed classical phase space consisting of regular islands embedded in the chaotic sea. For our considered case, the mixed classical phase space is present for $2 \lesssim \kappa \lesssim 5.4$. We thus fixed $\kappa = 3$ in our study. The mixed feature of the classical phase space for $\kappa = 3$ case can be visualized by the corresponding Poincaré section, as demonstrated in Fig. 1(c). We have numerically verified that our main conclusions still hold for other values of κ , as long as the corresponding classical dynamics is mixed. Moreover, a careful numerical check has shown that although the value of α can change the degree of chaos for both quantum and classical kicked top [101], it does not affect the main results of this work. This allows us to fix $\alpha = 13\pi/19$ in our study.

C. Mixed eigenstates

The mixed eigenstates, also referred to as hybridized states [26], are prevalent in generic quantum systems that have mixed classical phase space with coexistence of regular and chaotic motions. A prominent feature of the mixed eigenstates is manifested in their corresponding Husimi functions, distributing over both regular and chaotic regions. This means that the types of eigenstates are encoded in their corresponding Husimi functions.

For the k th eigenstate, $|\varepsilon_k\rangle$, of the Floquet operator, the Husimi function is given by [102]

$$Q_k(\theta, \phi) = |\langle \theta, \phi | \varepsilon_k \rangle|^2, \quad (6)$$

where

$$|\theta, \phi\rangle = e^{i\theta(S_x \sin \phi - S_y \cos \phi)} |S, S\rangle \quad (7)$$

are the SU(2) spin-coherent states [103, 104] localized at (θ, ϕ) and $S_z |S, S\rangle = S |S, S\rangle$. Moreover, the Husimi function $Q_k(\theta, \phi)$ is normalized as

$$\frac{2S+1}{4\pi} \int d\mathcal{A} Q_k(\theta, \phi) = 1, \quad (8)$$

with $d\mathcal{A} = \sin \theta d\theta d\phi$ being the area element on the unit sphere. To identify the types of the eigenstates, let us first discretize the Husimi function by dividing the classical phase space into a grid with $N \times N$ equal cells that are marked by their central points and are indexed as (p, q) with $p, q = 1, 2, \dots, N$. Then, we assign a value $C_{pq} = +1$ to the cells that reside in the chaotic region, and $C_{pq} = -1$ otherwise. Finally, the types of the k th eigenstate is determined by the phase space overlap index, which is defined as

$$\chi_k = \frac{2S+1}{4\pi} \sum_{p,q} Q_k(\theta_p, \phi_q) C_{pq} \Delta A_{pq}, \quad (9)$$

where ΔA_{pq} is the area of the cell with index (p, q) . The definition of χ_k leads to $-1 \leq \chi_k \leq 1$ with $\chi_k = -1$ and $+1$, respectively, corresponding to regular and fully chaotic eigenstates. Hence, the mixed eigenstates are identified as $\chi_k \neq \pm 1$.

In our numerical simulation, the chaotic region is generated by evolving an initial condition, which is randomly chosen from the chaotic region of phase space, up to 10^8 kicks. As a result, the complement includes all regular and possibly tiny chaotic regions. However, we can take the tiny chaotic regions as a part of regular region, as they are vanishingly small. Moreover, to ensure that the discretized Husimi function is normalized and our results are converged, we set $N \times N = 300 \times 300$ throughout this work. The Husimi function for several quasieigenstates of \mathcal{F} in (3) with associated χ_k are shown in Fig. 2. Comparing them to the corresponding Poincaré section, which we plot in Fig. 2(e), we see that in contrast to the regular and chaotic eigenstates, such as the one displayed in Figs. 2(a) and 2(d), the Husimi function of the mixed eigenstates spreads over both classical regular and chaotic regions. However, in the sufficiently deep semiclassical limit, the relative fraction of mixed-type eigenstates decays as a power law [24, 25, 28]. This prominent character of the mixed eigenstates leads us to expect that it should also get reflected in the dynamical behaviors of mixed eigenstates. In the following section, we investigate this question by means of the OTOC.

III. DYNAMICAL SIGNATURES OF THE MIXED EIGENSTATES

To analyze how the mixed feature of the mixed eigenstates manifests in their dynamical behaviors through the OTOC, we take the initial Hermitian operators as $A = s_x = S_x/S$ and $B = \rho_c = |\theta, \phi\rangle\langle \theta, \phi|$ with $|\theta, \phi\rangle$ being the spin

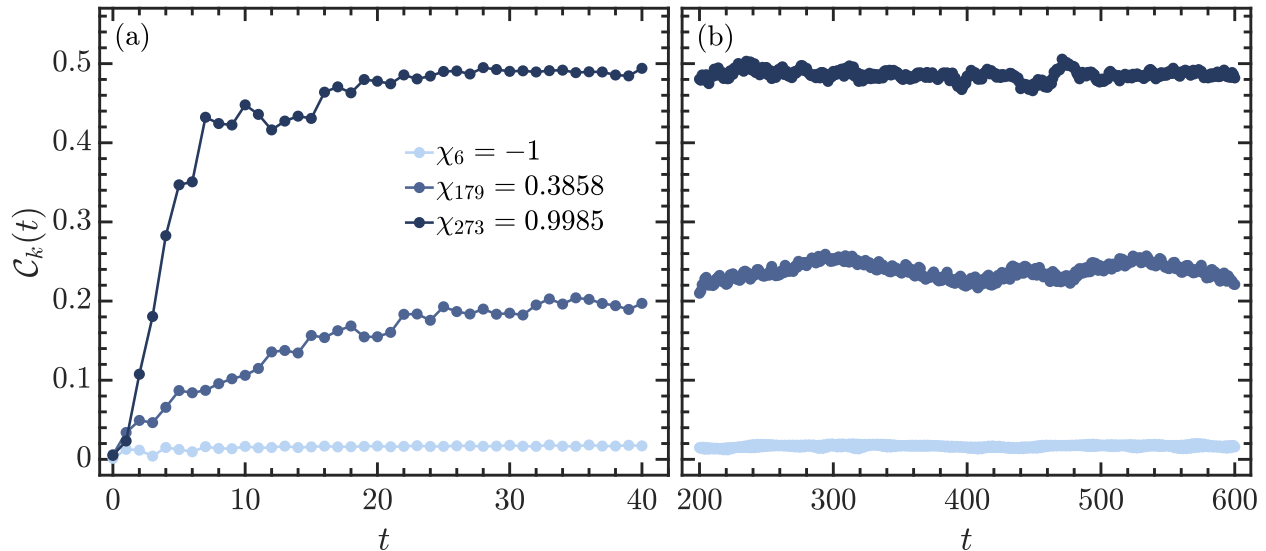


FIG. 4. Short-time (a) and long-time (b) phase space averaged OTOC, $C_k(t)$ in Eq. (15) for the eigenstates with corresponding values of χ_k are given in the legend of panel(a). Other parameters: $\alpha = 13\pi/19$, $\kappa = 3$, and the system size $S = 150$.

coherent state in (7). Then, for the k th eigenstate $|\varepsilon_k\rangle$, the OTOC is given by

$$c_k(t) = \langle \varepsilon_k | [s_x(t), \rho_c]^\dagger [s_x(t), \rho_c] | \varepsilon_k \rangle = c_{k,1}(t) - c_{k,2}(t), \quad (10)$$

where $c_{k,1}(t) = \langle x(t)|x(t)\rangle + \langle y(t)|y(t)\rangle$ and $c_{k,2}(t) = \langle x(t)|y(t)\rangle + \langle y(t)|x(t)\rangle$. Here, we have defined $|x(t)\rangle = s_x(t)\rho_c|\varepsilon_k\rangle$ and $|y(t)\rangle = \rho_c s_x(t)|\varepsilon_k\rangle$ with $s_x(t) = \mathcal{F}^\dagger t S_x \mathcal{F}^t / S$. The reason for choosing density operator of the coherent states is that it allows us to understand how the mixed structure in the phase space affects the evolution of the eigenstate OTOC. However, the choice of s_x is not unique. In fact, we have checked that the results obtained for s_x also hold for other operators, such as $s_y = S_y/S$, as long as they do not commute with the Floquet operator. Otherwise, the OTOC would be independent of the time.

The role played by the type of the eigenstates for the behavior of $c_k(t)$ cannot be directly unveiled by Eq. (10). To uncover how the type of the eigenstates get reflected in the evolution of $c_k(t)$, we derive an upper bound of $c_k(t)$ in terms of the Husimi function of the k th eigenstate. By using the closure relation of the eigenstates and spin coherent states,

$$\sum_u |\varepsilon_u\rangle \langle \varepsilon_u| = 1, \quad \frac{2S+1}{4\pi} \int d\mathcal{A} |\theta, \phi\rangle \langle \theta, \phi| = 1, \quad (11)$$

we first rewrite $c_k(t)$ as

$$c_k(t) = \sum_u |\langle \varepsilon_u | \mathcal{O}(t) | \varepsilon_k \rangle|^2 = \left(\frac{2S+1}{4\pi} \right)^2 \sum_u \left| \int d\mathcal{A}_1 \langle \varepsilon_u | \mathcal{O}(t) | \theta_1, \phi_1 \rangle \langle \theta_1, \phi_1 | \varepsilon_k \rangle \right|^2, \quad (12)$$

where $\mathcal{O}(t) = [s_x(t), \rho_c]$ is the commutator between $s_x(t)$ and ρ_c . Then, the Cauchy-Schwarz inequality leads us to obtain

$$\begin{aligned} \left| \int d\mathcal{A}_1 \langle \varepsilon_u | \mathcal{O}(t) | \theta_1, \phi_1 \rangle \langle \theta_1, \phi_1 | \varepsilon_k \rangle \right|^2 &\leq \left(\int d\mathcal{A}_1 1^2 \right) \left(\int d\mathcal{A}_1 |\langle \varepsilon_u | \mathcal{O}(t) | \theta_1, \phi_1 \rangle|^2 Q_k(\theta_1, \phi_1) \right) \\ &= 4\pi \int d\mathcal{A}_1 Q_k(\theta_1, \phi_1) |\langle \varepsilon_u | \mathcal{O}(t) | \theta_1, \phi_1 \rangle|^2, \end{aligned} \quad (13)$$

where $\int d\mathcal{A}_1 = 4\pi$ has been employed and $Q_k(\theta_1, \phi_1)$ denotes the Husimi function in Eq. (6). As a result, we finally

find that $c_k(t)$ is upper bounded by

$$\begin{aligned} c_k(t) &\leq \frac{(2S+1)^2}{4\pi} \int d\mathcal{A}_1 Q_k(\theta_1, \phi_1) \sum_u \langle \theta_1, \phi_1 | \mathcal{O}^\dagger(t) | \varepsilon_u \rangle \langle \varepsilon_u | \mathcal{O}(t) | \theta_1, \phi_1 \rangle \\ &= \frac{(2S+1)^2}{4\pi} \int d\mathcal{A}_1 Q_k(\theta_1, \phi_1) \mathcal{W}_t(\theta_1, \phi_1), \end{aligned} \quad (14)$$

where $\mathcal{W}_t(\theta_1, \phi_1) = \langle \theta_1, \phi_1 | \mathcal{O}^\dagger(t) \mathcal{O}(t) | \theta_1, \phi_1 \rangle$ is the OTOC with respect to the spin coherent states. Here, the last equality is obtained by using the closure relation of the eigenstates in (11).

It is known that the OTOC is less prone to scrambling for the coherent states located in the regular regions, while it exhibits a fast spreading over the chaotic sea for the coherent states resided in the chaotic component [61, 78]. Then, according to the inequality of (14), $c_k(t)$ will evolve in the regular regions for the regular eigenstates and it should undergo a rapid expanding in the chaotic region for chaotic eigenstates. However, as the Husimi function of the mixed eigenstates occupies both regular and chaotic regions, the evolution of $c_k(t)$ will display some mixed features for the mixed eigenstates. In other words, the time dependence of $c_k(t)$ for the mixed eigenstates is a combination of the restricting motion in the regular regions and an extending in the chaotic region.

In Fig. 3, we plot $c_k(t)$ in classical phase space at different time steps for regular, mixed, and chaotic eigenstates, respectively. The dependence of the behavior of $c_k(t)$ on the type of eigenstate is clearly visible. Specifically, as seen in Figs. 3(a1)-3(a4), the evolution of OTOC for the regular state is confined within the regular region. On the contrary, the OTOC spreads over the chaotic region for the chaotic eigenstate, as demonstrated in Figs. 3(c1)-3(c4). Distinct from both regular and chaotic eigenstates, as observed in Figs. 3(b1)-3(b4), the OTOC of the mixed eigenstate is initially evolved in the regular region and gradually spread into the chaotic region with increasing time. These results suggest that the type of the eigenstates leaves an imprint on the behavior of OTOC.

Further dynamical properties of the mixed eigenstates can be quantitatively revealed by the phase space averaged OTOC, which is defined as

$$\mathcal{C}_k(t) = \frac{2S+1}{4\pi} \int c_k(t) \sin \theta d\theta d\phi. \quad (15)$$

The results in Fig. 3 indicate that the time dependence of $\mathcal{C}_k(t)$ should be strongly correlated with the type of eigenstate. This is verified in Fig. 4, where we show the short-time and long-time evolutions of $\mathcal{C}_k(t)$ for the regular, mixed, and chaotic eigenstates. The confining behavior of $c_k(t)$ for the regular state results in $\mathcal{C}_k(t)$ evolving around a vanishingly small value with almost no fluctuations. In contrast, due to the fast spreading of $c_k(t)$ in the phase space, $\mathcal{C}_k(t)$ of the chaotic state starts with a rapid growth followed by tiny fluctuations around certain saturation value. In particular, one can observe that the behavior of $\mathcal{C}_k(t)$ for the mixed eigenstate is very different from the regular and chaotic states. As the mixed eigenstate exhibits a slow extending of $c_k(t)$ over the phase space, the corresponding $\mathcal{C}_k(t)$ increases with a lower rate and it eventually saturates with small oscillations at long time. The saturation value of $\mathcal{C}_k(t)$ for the mixed eigenstate is smaller compared to the chaotic state and it should depend on the value of χ_k . Moreover, we further note that the initial growth rate of $\mathcal{C}_k(t)$ also correlates to χ_k . These results imply that the dynamical signatures of the mixed eigenstates are encoded in both short- and long-time properties of $\mathcal{C}_k(t)$.

A. Short-time growth rate of phase space averaged OTOC

To analyze how the mixed eigenstates manifest themselves in the short-time behavior of $\mathcal{C}_k(t)$, we define its initial growth rate as

$$\gamma_k = \frac{\mathcal{C}_k(\tau) - \mathcal{C}_k(0)}{\tau} \simeq \frac{d\mathcal{C}_k(\tau)}{d\tau}, \quad (16)$$

where τ is the final time of the initial growth. It was known that OTOCs usually exhibit a growth until the Ehrenfest time $t_E \sim \log(\mathcal{D}_{\mathcal{H}})/\lambda_{cl}$ with $\mathcal{D}_{\mathcal{H}}$ and λ_{cl} are, respectively, the Hilbert space dimension and the classical Lyapunov exponent. As λ_{cl} has the order of magnitude $O(1)$ for our considered case, we thus take $\tau = \lfloor \ln(2S+1) \rfloor$ in the numerical calculations. Here, $\lfloor x \rfloor$ means the nearest integer of x .

The results in Fig. 4 indicate that γ_k is defined in an interval $\gamma_k \in [\gamma_{k,min}, \gamma_{k,max}]$. For regular eigenstates, we have $\gamma_k = \gamma_{k,min} \sim 0$, while $\gamma_k = \gamma_{k,max}$ corresponding to the chaotic eigenstates. The value of γ_k for the mixed eigenstates varies in between.

In Figs. 5(a) and 5(b), we show the scatter plots of γ and χ of the eigenstates for different system sizes. As expected, we see that the regular and chaotic eigenstates have the values of γ that are clustered around its minimal and maximal

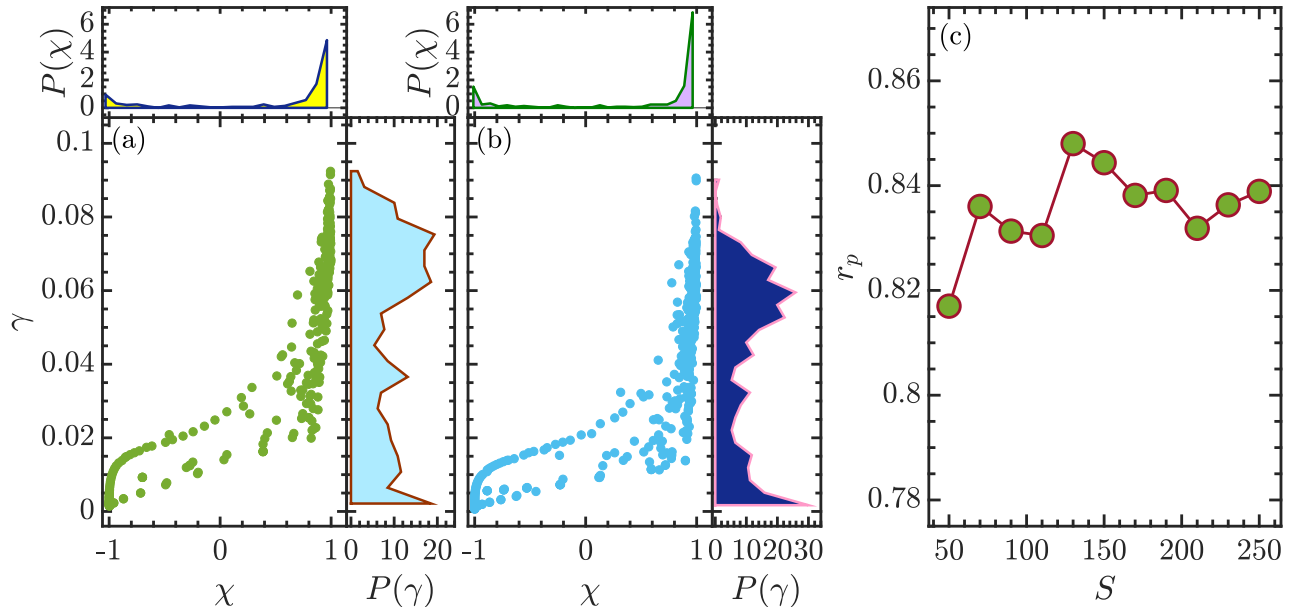


FIG. 5. Scatter plots of γ versus χ for the system size (a) $S = 150$ and (b) $S = 250$. The top and right panels in (a) and (b) are, respectively, plotted the probability distributions $P(\chi)$ and $P(\gamma)$, defined in Eq. (17). (c) Pearson product-momentum correlation coefficient r_p in Eq. (18) of χ_k and γ_k as a function of system size S . Other parameters: $\alpha = 13\pi/19$, $\kappa = 3$.

value, regardless of the system size. For the mixed eigenstates with $-1 < \chi < 1$, the initial growth rate γ exhibits a wide distribution between two extreme values, indicating that the value of γ can be used to characterize the degree of mixture of the mixed eigenstates.

To further show how the mixed eigenstates are correlated with γ , we consider the probability distributions of γ and χ , which are defined as

$$P(\gamma) = \frac{1}{2S+1} \sum_{\gamma_k} \delta(\gamma - \gamma_k), \quad P(\chi) = \frac{1}{2S+1} \sum_{\chi_k} \delta(\chi - \chi_k), \quad (17)$$

where S is the magnitude of the angular momentum and also denotes the system size. Our previous works [24, 25] have demonstrated that $P(\chi)$ has the double peak shape with two peaks corresponding to regular and chaotic eigenstates, respectively. Consequently, one can expect that the shape of $P(\gamma)$ should also be the double peak. This is verified in top and right panels of Fig. 5(a) and 5(b), where the probability distribution $P(\gamma)$ and $P(\chi)$ are displayed. However, we note that $P(\gamma)$ is supported on a much smaller interval than $P(\chi)$, which leads to a less sharp double peak in $P(\gamma)$ as compared to $P(\chi)$. Nevertheless, we observe that the sharpness of the double peak shape in $P(\chi)$ can be enhanced as the system size is increased. It is worth pointing out that this enhancement also implies the decreasing of the relative fraction of the mixed eigenstates with increasing the system size, consisting with our previous result [24, 28].

The quality of the correlation can be quantitatively measured by the correlation coefficient. For the two random variables $\{(U_i, V_i)\}$, the dependence between them is usually quantified by the well-known Pearson product-moment correlation coefficient [105], defined by

$$r_p = \frac{\sum_i (U_i - \bar{U})(V_i - \bar{V})}{\sqrt{\sum_i (U_i - \bar{U})^2 \sum_i (V_i - \bar{V})^2}}, \quad (18)$$

where \bar{U} and \bar{V} are the average of U_i and V_i , respectively. The Pearson coefficient r_P for our case is calculated by replacing (U_i, V_i) with (χ_k, γ_k) . In Fig. 5(c), we plot how r_P varies with increasing the system size S . It is obvious that r_P has a larger value $r_P \approx 0.84$ almost independent of the system size. This feature confirms the strong correlation between γ and χ . It also prompts us to conjecture that the short time growth rate of the phase space averaged OTOC reflects the dynamical character of the mixed eigenstates.

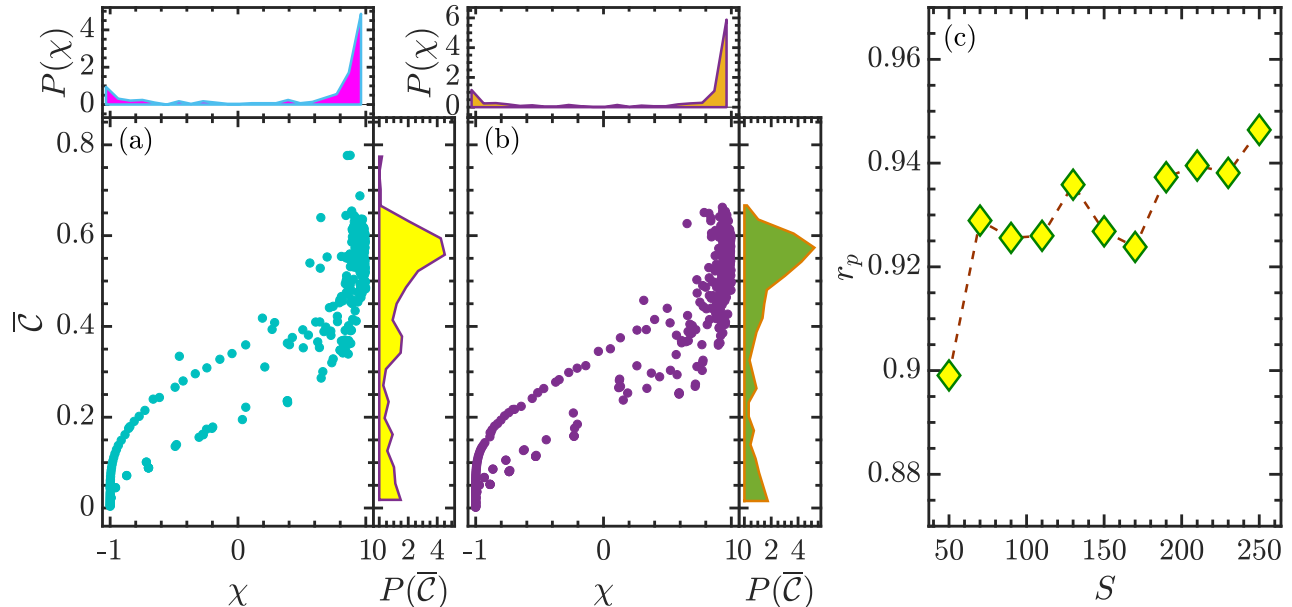


FIG. 6. Scatter plots of \bar{C} as a function of χ for the system size (a) $S = 150$ and (b) $S = 250$. The top and right panels in (a) and (b) are, respectively, plotted the probability distributions $P(\chi)$ in Eq. (17) and $P(\bar{C})$ in Eq. (23). (c) Pearson product-momentum correlation coefficient r_p , defined in Eq. (18), of \bar{C}_k and χ_k as a function of system size S . Other parameters: $\alpha = 13\pi/19$, $\kappa = 3$.

B. Long-time average of phase space averaged OTOC

The dynamical signature of the mixed eigenstates can also be revealed by the long-time average of $C_k(t)$, defined as

$$\bar{C}_k = \lim_{T \rightarrow \infty} \frac{1}{T} \int_t^{t+T} C_k(v) dv, \quad (19)$$

where $t \gg 1$ should be sufficiently larger than the initial time scale. In our numerical simulations, we take $t = 100$ and $T = 500$. We have carefully checked that further increasing t and T does not change our main results. By inserting Eq. (15) into (19), after some algebra, one gets

$$\bar{C}_k = \frac{2S+1}{4\pi} \int \bar{c}_k \sin \theta d\theta d\phi, \quad (20)$$

where

$$\bar{c}_k = \lim_{T \rightarrow \infty} \frac{1}{T} \int_t^{t+T} c_k(v) dv = C_{k,1} - 2C_{k,2}, \quad (21)$$

and

$$\begin{aligned} C_{k,1} &= Q_k \sum_p Q_p (s_x)_{pp} + \sum_p Q_p (s_x)_{kp} (s_x)_{pk} - 2(s_x)_{kk}^2 Q_k^4, \\ C_{k,2} &= Q_k \sum_{p \neq k} [Q_p (s_x)_{pp} (s_x)_{kk} + Q_p (s_x)_{kp} (s_x)_{pk}], \end{aligned} \quad (22)$$

with Q_k being the Husimi function (6) of the k th eigenstate and $(s_x)_{ab} = \langle \varepsilon_a | S_x | \varepsilon_b \rangle / S$. Here, the integration in Eq. (21) has been carried out by assuming that the energy spectrum has no degeneracies.

It is known that the fully chaotic eigenstates are almost uniformly distributed over a given basis. As a result, we have $C_{k,1} \sim O(1/S)$ and $C_{k,2} \sim O(1/S^2)$, suggesting $\bar{c}_k \sim O(1/S)$ and $\bar{C}_{k,max} \sim O(1)$. For the regular eigenstates, $C_{k,1}$ and $C_{k,2}$ have the same order of magnitude $O(1/S^2)$, leading to $\bar{C}_{k,min} \sim O(1/S)$. However, as the mixed eigenstates

are partially localized in the regular region and partially extended in the chaotic region, one can reasonably expect that the values of their \bar{C}_k are directly linked to χ_k and vary from $\bar{C}_{k,min}$ to $\bar{C}_{k,max}$.

The scatter plots of \bar{C}_k versus χ for all eigenstates with different system sizes are shown in Figs. 6(a) and 6(b). An overall similarity between Figs. 6(a)-6(b) and Figs. 5(a)-5(b) is clearly visible. We see that \bar{C} clusters around its minimal and maximal values which are, respectively, corresponding to the regular and chaotic eigenstates, as indicated by the value of χ . Besides, one can further observe that the mixed eigenstates with $-1 < \chi < 1$ have values of \bar{C}_k that are scattered between two clusters. These results confirm that the types of the eigenstates have strong impact on evolution of the OTOC, and the unique features in the OTOC exhibited by the mixed eigenstates enable us to distinguish them from chaotic and regular eigenstates.

To further uncover the links between the long-time averaged OTOC and the signatures of mixed eigenstates, we consider the probability distribution of \bar{C}_k , defined by

$$P(\bar{C}) = \frac{1}{2S+1} \sum_k \delta(\bar{C} - \bar{C}_k), \quad (23)$$

and compare it to $P(\chi)$ in Eq. (17). The results for different systems are plotted in the right and top panels of Figs. 6(a) and 6(b). We first note that $P(\bar{C})$ has a similar shape as $P(\chi)$, regardless of the system size. Both $P(\bar{C})$ and $P(\chi)$ are characterized by double peak distribution with two peaks corresponding to regular and chaotic eigenstates, respectively. The mixed eigenstates are marked by smaller values of $P(\bar{C})$ and $P(\chi)$ that are distributed between two peaks. In particular, we observe that the double peak shape of $P(\bar{C})$ and $P(\chi)$ become sharper as the system size is increased. This is in agreement with the expectation that the relative fraction of the mixed eigenstates decreases with increasing the system size [23–25, 27, 28].

The remarkable agreements exhibited by $P(\bar{C})$ and $P(\chi)$ indicate the equivalence between them. To confirm this statement, we study the correlation coefficient between \bar{C}_k and χ_k , calculated by r_p in Eq. (18) with (\bar{C}_k, χ_k) serving as (U_i, V_i) . In Fig. 6(c), we plot how r_p varies as a function of the system size S . We see that r_p shows a weak dependence on the system size and it displays only a small fluctuation around $r_p \approx 0.93$ with increasing S . This not only demonstrates that the behavior of the long-time averaged OTOC is strongly correlated with the types of the eigenstates, but also verifies that the OTOC acts as a valuable tool to analyze the dynamical signatures of the mixed eigenstates. Moreover, one can observe that r_p in Fig. 6(c) is larger than the one in Fig. 5(c), suggesting that the long-time averaged OTOC is more reliable to distinguish the mixed eigenstates than the initial growth rate of the OTOC.

IV. CONCLUSIONS

In conclusion, we have examined the dynamical signatures of the mixed eigenstates in a mixed-type system. Different from regular and fully chaotic systems, a mixed-type system has mixed phase space with regular islands embedded in chaotic sea. This led Percival to classify quantum spectra of the mixed-type systems into regular and chaotic types [12]. However, this binary classification is an idealization and the quantum eigenstates in the actual situations are more complex. In fact, it has been found that the mixed eigenstates with Husimi function occupying both regular and chaotic regions are more prevalent in the mixed-type systems. Hence, studying the properties of the mixed eigenstates is crucial for understanding various phenomena exhibited by the mixed-type systems. Previous works have investigated the statistical features of the mixed eigenstates [26] and had numerically verified that their relative fraction in the semiclassical limit decreases according to a power law [23–25, 27, 28]. In this work, we have demonstrated how to characterize the mixed eigenstates through the dynamics of the OTOC in the kicked top model, which behaves as a mixed-type system for certain control parameters.

The mixed eigenstates in our study are identified using the phase space overlap index, which measures the degree of the mixture of the eigenstates and has been employed in our previous works [23–25, 27, 28]. We have shown that the time dependence of OTOC for the mixed eigenstates exhibits unique behavior which distinguishes the cases of regular and chaotic eigenstates. In particular, the short- and long-time behaviors of OTOC exhibit an obvious dependence on the degree of the mixture of the eigenstates. This has led us to analyze the dynamical characters of the mixed eigenstates through the initial growth rate and long-time average of the OTOC, respectively. We have revealed how the initial growth rate and long-time average of OTOC connect to the phase space overlap index and quantified their correlations via the Pearson product-moment correlation coefficient.

Our findings offer further insights into the features of mixed eigenstates and also provide a comprehensive perspective on the mixed-type systems. As the mixed eigenstates are commonly described by the distribution of their Husimi function in both regular and chaotic regions, we expect that the main conclusions of this work may still hold for other mixed-type systems. It would be interesting to systematically study dynamical properties of the mixed eigenstates

in various mixed-type systems, such as billiards and Dicke model, via the OTOCs. Another question that deserves future exploring is to find an analytical explanation for our numerical results. Moreover, the OTOCs have been experimentally measured in a variety of platforms [57–60]. This led us to further expect that our work could stimulate more experimental studies of dynamics in mixed-type systems.

ACKNOWLEDGMENTS

This work was supported by the Slovenian Research and Innovation Agency (ARIS) under the Grants Nos. J1-4387 and P1-0306.

-
- [1] A. K. Das and A. Ghosh, *Journal of Physics A: Mathematical and Theoretical* **56**, 495003 (2023).
 - [2] Z. D. Shi, S. Vardhan, and H. Liu, *Phys. Rev. B* **108**, 224305 (2023).
 - [3] A. P. Luca D’Alessio, Yariv Kafri and M. Rigol, *Advances in Physics* **65**, 239 (2016).
 - [4] E. J. Torres-Herrera and L. F. Santos, *The European Physical Journal Special Topics* **227**, 1897 (2019).
 - [5] M. Pandey, P. W. Claeys, D. K. Campbell, A. Polkovnikov, and D. Sels, *Phys. Rev. X* **10**, 041017 (2020).
 - [6] R. Nandkishore and D. A. Huse, *Annual Review of Condensed Matter Physics* **6**, 15 (2015).
 - [7] D. A. Abanin, E. Altman, I. Bloch, and M. Serbyn, *Rev. Mod. Phys.* **91**, 021001 (2019).
 - [8] I. M. Georgescu, S. Ashhab, and F. Nori, *Rev. Mod. Phys.* **86**, 153 (2014).
 - [9] A. J. Daley, I. Bloch, C. Kokail, S. Flannigan, N. Pearson, M. Troyer, and P. Zoller, *Nature* **607**, 667 (2022).
 - [10] V. Giovannetti, S. Lloyd, and L. Maccone, *Nature Photonics* **5**, 222 (2011).
 - [11] T. B. Magdalena Szczykulska and A. Datta, *Advances in Physics: X* **1**, 621 (2016).
 - [12] I. C. Percival, *Journal of Physics B: Atomic and Molecular Physics* **6**, L229 (1973).
 - [13] E. B. Stechel and E. J. Heller, *Annual Review of Physical Chemistry* **35**, 563 (1984).
 - [14] M. V. Berry, *Journal of Physics A: Mathematical and General* **10**, 2083 (1977).
 - [15] M. V. Berry and J. M. Ziman, *Philosophical Transactions of the Royal Society of London. Series A, Mathematical and Physical Sciences* **287**, 237 (1977).
 - [16] M. Robnik, “Topics in quantum chaos of generic systems,” (2000), arXiv:nlin/0003058 [nlin.CD].
 - [17] M. V. Berry and M. Robnik, *Journal of Physics A: Mathematical and General* **17**, 2413 (1984).
 - [18] M. Robnik, *Nonlinear Phenomena in Complex Systems* **23**, 172 (2020).
 - [19] M. Robnik, *Interdisciplinary Journal Nonlinear Phenomena in Complex Systems* **26** (2024), 10.5281/zenodo.10030989.
 - [20] S. Tomsovic and D. Ullmo, *Phys. Rev. E* **50**, 145 (1994).
 - [21] S. D. Frischat and E. Doron, *Phys. Rev. E* **57**, 1421 (1998).
 - [22] S. Löck, A. Bäcker, R. Ketzmerick, and P. Schlagheck, *Phys. Rev. Lett.* **104**, 114101 (2010).
 - [23] Č. Lozej, D. Lukman, and M. Robnik, *Phys. Rev. E* **106**, 054203 (2022).
 - [24] Q. Wang and M. Robnik, *Phys. Rev. E* **108**, 054217 (2023).
 - [25] Q. Wang and M. Robnik, *Phys. Rev. E* **109**, 024225 (2024).
 - [26] A. V. Varma, A. Vardi, and D. Cohen, *Phys. Rev. E* **109**, 064207 (2024).
 - [27] H. Yan and M. Robnik, *Phys. Rev. E* **109**, 054211 (2024).
 - [28] H. Yan, Q. Wang, and M. Robnik, *Phys. Rev. E* **110**, 064222 (2024).
 - [29] S. Xu and B. Swingle, *Phys. Rev. X* **9**, 031048 (2019).
 - [30] J. R. González Alonso, N. Yunger Halpern, and J. Dressel, *Phys. Rev. Lett.* **122**, 040404 (2019).
 - [31] B. Yan, L. Cincio, and W. H. Zurek, *Phys. Rev. Lett.* **124**, 160603 (2020).
 - [32] S. Xu and B. Swingle, *PRX Quantum* **5**, 010201 (2024).
 - [33] A. I. Larkin and Y. N. Ovchinnikov, *Sov Phys JETP* **28**, 1200 (1969).
 - [34] X. Chen, T. Zhou, D. A. Huse, and E. Fradkin, *Annalen der Physik* **529**, 1600332 (2017).
 - [35] R. Fan, P. Zhang, H. Shen, and H. Zhai, *Science Bulletin* **62**, 707 (2017).
 - [36] B. Dóra and R. Moessner, *Phys. Rev. Lett.* **119**, 026802 (2017).
 - [37] C.-J. Lin and O. I. Motrunich, *Phys. Rev. B* **97**, 144304 (2018).
 - [38] S. H. Shenker and D. Stanford, *Journal of High Energy Physics* **2014**, 67 (2014).
 - [39] J. Maldacena, S. H. Shenker, and D. Stanford, *Journal of High Energy Physics* **2016**, 106 (2016).
 - [40] E. B. Rozenbaum, S. Ganesan, and V. Galitski, *Phys. Rev. Lett.* **118**, 086801 (2017).
 - [41] I. García-Mata, M. Saraceno, R. A. Jalabert, A. J. Roncaglia, and D. A. Wisniacki, *Phys. Rev. Lett.* **121**, 210601 (2018).
 - [42] J. Chávez-Carlos, B. López-del Carpio, M. A. Bastarrachea-Magnani, P. Stránský, S. Lerma-Hernández, L. F. Santos, and J. G. Hirsch, *Phys. Rev. Lett.* **122**, 024101 (2019).
 - [43] R. J. Lewis-Swan, A. Safavi-Naini, J. J. Bollinger, and A. M. Rey, *Nature Communications* **10**, 1581 (2019).
 - [44] I. L. Aleiner, L. Faoro, and L. B. Ioffe, *Annals of Physics* **375**, 378 (2016).
 - [45] J. S. Cotler, D. Ding, and G. R. Penington, *Annals of Physics* **396**, 318 (2018).
 - [46] E. M. Fortes, I. García-Mata, R. A. Jalabert, and D. A. Wisniacki, *Phys. Rev. E* **100**, 042201 (2019).

- [47] T. Xu, T. Scaffidi, and X. Cao, *Phys. Rev. Lett.* **124**, 140602 (2020).
- [48] W. Kirkby, D. H. J. O'Dell, and J. Mumford, *Phys. Rev. A* **104**, 043308 (2021).
- [49] N. Dowling, P. Kos, and K. Modi, *Phys. Rev. Lett.* **131**, 180403 (2023).
- [50] E. B. Rozenbaum, S. Ganeshan, and V. Galitski, *Phys. Rev. B* **100**, 035112 (2019).
- [51] M. Rautenberg and M. Gärttner, *Phys. Rev. A* **101**, 053604 (2020).
- [52] J. R. G. Alonso, N. Shammah, S. Ahmed, F. Nori, and J. Dressel, "Diagnosing quantum chaos with out-of-time-ordered-correlator quasiprobability in the kicked-top model," (2022), arXiv:2201.08175 [quant-ph].
- [53] D. A. Trunin, *Phys. Rev. D* **108**, 105023 (2023).
- [54] J. Novotný and P. Stránský, *Phys. Rev. E* **107**, 054220 (2023).
- [55] I. García-Mata, R. A. Jalabert, and D. A. Wisniacki, *Scholarpedia* **18**, 55237 (2023), revision #199677.
- [56] R. K. Shukla, G. R. Malik, S. Aravinda, and S. K. Mishra, "Discriminating chaotic and integrable regimes in quenched field floquet system using saturation of out-of-time-order correlation," (2024), arXiv:2404.04177 [quant-ph].
- [57] J. Li, R. Fan, H. Wang, B. Ye, B. Zeng, H. Zhai, X. Peng, and J. Du, *Phys. Rev. X* **7**, 031011 (2017).
- [58] M. Gärttner, J. G. Bohnet, A. Safavi-Naini, M. L. Wall, J. J. Bollinger, and A. M. Rey, *Nature Physics* **13**, 781 (2017).
- [59] J. Braumüller, A. H. Karamlou, Y. Yanay, B. Kannan, D. Kim, M. Kjaergaard, A. Melville, B. M. Niedzielski, Y. Sung, A. Vepsäläinen, R. Winik, J. L. Yoder, T. P. Orlando, S. Gustavsson, C. Tahan, and W. D. Oliver, *Nature Physics* **18**, 172 (2022).
- [60] A. M. Green, A. Elben, C. H. Alderete, L. K. Joshi, N. H. Nguyen, T. V. Zache, Y. Zhu, B. Sundar, and N. M. Linke, *Phys. Rev. Lett.* **128**, 140601 (2022).
- [61] P. D. Blocher, S. Asaad, V. Mourik, M. A. I. Johnson, A. Morello, and K. Mølmer, *Phys. Rev. A* **106**, 042429 (2022).
- [62] N. Lashkari, D. Stanford, M. Hastings, T. Osborne, and P. Hayden, *Journal of High Energy Physics* **2013**, 22 (2013).
- [63] I. Kukuljan, S. Grozdanov, and T. Prosen, *Phys. Rev. B* **96**, 060301 (2017).
- [64] T. Schuster, M. Niu, J. Cotler, T. O'Brien, J. R. McClean, and M. Mohseni, *Phys. Rev. Res.* **5**, 043284 (2023).
- [65] K. Hashimoto, K. Murata, and R. Yoshii, *Journal of High Energy Physics* **2017**, 138 (2017).
- [66] H. Yan, J.-Z. Wang, and W.-G. Wang, *Communications in Theoretical Physics* **71**, 1359 (2019).
- [67] S. Pilatowsky-Cameo, J. Chávez-Carlos, M. A. Bastarrachea-Magnani, P. Stránský, S. Lerma-Hernández, L. F. Santos, and J. G. Hirsch, *Phys. Rev. E* **101**, 010202 (2020).
- [68] E. B. Rozenbaum, L. A. Bunimovich, and V. Galitski, *Phys. Rev. Lett.* **125**, 014101 (2020).
- [69] K. Hashimoto, K.-B. Huh, K.-Y. Kim, and R. Watanabe, *Journal of High Energy Physics* **2020**, 68 (2020).
- [70] J. Wang, G. Benenti, G. Casati, and W.-g. Wang, *Phys. Rev. E* **103**, L030201 (2021).
- [71] A. Lakshminarayan, *Phys. Rev. E* **99**, 012201 (2019).
- [72] E. J. Torres-Herrera, A. M. García-García, and L. F. Santos, *Phys. Rev. B* **97**, 060303 (2018).
- [73] J. Rammensee, J. D. Urbina, and K. Richter, *Phys. Rev. Lett.* **121**, 124101 (2018).
- [74] P. D. Bergamasco, G. G. Carlo, and A. M. F. Rivas, *Phys. Rev. Res.* **1**, 033044 (2019).
- [75] F. Borgonovi, F. M. Izrailev, and L. F. Santos, *Phys. Rev. E* **99**, 052143 (2019).
- [76] J. Riddell, W. Kirkby, D. H. J. O'Dell, and E. S. Sørensen, *Phys. Rev. B* **108**, L121108 (2023).
- [77] V. Balachandran, L. F. Santos, M. Rigol, and D. Poletti, *Phys. Rev. B* **107**, 235421 (2023).
- [78] N. D. Varikuti and V. Madhok, *Chaos: An Interdisciplinary Journal of Nonlinear Science* **34**, 063124 (2024).
- [79] S. V. Syzranov, A. V. Gorshkov, and V. Galitski, *Phys. Rev. B* **97**, 161114 (2018).
- [80] A. K. Chatterjee, A. Kundu, and M. Kulkarni, *Phys. Rev. E* **102**, 052103 (2020).
- [81] L.-J. Zhai and S. Yin, *Phys. Rev. B* **102**, 054303 (2020).
- [82] W.-L. Zhao, *Phys. Rev. Res.* **4**, 023004 (2022).
- [83] P. D. Bergamasco, G. G. Carlo, and A. M. F. Rivas, *Phys. Rev. E* **108**, 024208 (2023).
- [84] R. A. Kidd, A. Safavi-Naini, and J. F. Corney, *Phys. Rev. A* **103**, 033304 (2021).
- [85] M. Brenes, S. Pappalardi, M. T. Mitchison, J. Gould, and A. Silva, *Phys. Rev. E* **104**, 034120 (2021).
- [86] M. Heyl, F. Pollmann, and B. Dóra, *Phys. Rev. Lett.* **121**, 016801 (2018).
- [87] Q. Wang and F. Pérez-Bernal, *Phys. Rev. A* **100**, 062113 (2019).
- [88] X. Nie, B.-B. Wei, X. Chen, Z. Zhang, X. Zhao, C. Qiu, Y. Tian, Y. Ji, T. Xin, D. Lu, and J. Li, *Phys. Rev. Lett.* **124**, 250601 (2020).
- [89] B. Chen, X. Hou, F. Zhou, P. Qian, H. Shen, and N. Xu, *Applied Physics Letters* **116**, 194002 (2020).
- [90] K.-B. Huh, K. Ikeda, V. Jahnke, and K.-Y. Kim, *Phys. Rev. E* **104**, 024136 (2021).
- [91] S. Zamani, R. Jafari, and A. Langari, *Phys. Rev. B* **105**, 094304 (2022).
- [92] Q. Bin, L.-L. Wan, F. Nori, Y. Wu, and X.-Y. Lü, *Phys. Rev. B* **107**, L020202 (2023).
- [93] F. Haake, S. Gnutzmann, and M. Kuś, *Quantum Signatures of Chaos*, Springer Series in Synergetics (Springer International Publishing, 2019).
- [94] S. Chaudhury, A. Smith, B. E. Anderson, S. Ghose, and P. S. Jessen, *Nature* **461**, 768 (2009).
- [95] C. Neill, P. Roushan, M. Fang, Y. Chen, M. Kolodrubetz, Z. Chen, A. Megrant, R. Barends, B. Campbell, B. Chiaro, A. Dunsworth, E. Jeffrey, J. Kelly, J. Mutus, P. J. J. O'Malley, C. Quintana, D. Sank, A. Vainsencher, J. Wenner, T. C. White, A. Polkovnikov, and J. M. Martinis, *Nature Physics* **12**, 1037 (2016).
- [96] V. R. Krithika, V. S. Anjusha, U. T. Bhosale, and T. S. Mahesh, *Phys. Rev. E* **99**, 032219 (2019).
- [97] E. J. Meier, J. Ang'ong'a, F. A. An, and B. Gadway, *Phys. Rev. A* **100**, 013623 (2019).
- [98] A. Piga, M. Lewenstein, and J. Q. Quach, *Phys. Rev. E* **99**, 032213 (2019).
- [99] M. H. Muñoz Arias, P. M. Poggi, and I. H. Deutsch, *Phys. Rev. E* **103**, 052212 (2021).
- [100] Q. Wang and M. Robnik, *Phys. Rev. E* **107**, 054213 (2023).

- [101] Q. Wang and M. Robnik, *Entropy* **23** (2021), 10.3390/e23101347.
- [102] K. Husimi, *Nippon Sugaku-Buturigakkwai Kizi Dai 3 Ki* **22**, 264 (1940).
- [103] A. M. Perelomov, *Soviet Physics Uspekhi* **20**, 703 (1977).
- [104] W.-M. Zhang, D. H. Feng, and R. Gilmore, *Rev. Mod. Phys.* **62**, 867 (1990).
- [105] J. Sneyd, R. Fewster, and D. McGillivray, *Mathematics and Statistics for Science* (Springer International Publishing, 2022).